

Multiaxial high-cycle fatigue criterion and life prediction for metals

Yongming Liu, Sankaran Mahadevan*

Department of Civil and Environmental Engineering, Vanderbilt University, P.O. Box 1831-B, Nashville, TN 37235, USA

Received 26 August 2004; received in revised form 9 November 2004; accepted 10 January 2005

Abstract

A new high-cycle fatigue criterion based on the critical plane approach is proposed in this paper. Unlike most of the other multiaxial fatigue criteria based on the critical plane approach, the critical plane is directly correlated with the fatigue fracture plane. The proposed criterion has a wide range of applicability from very ductile metals to extremely brittle metals. Mean stress effect is also included in this criterion. The new fatigue criterion is then extended to a fatigue life prediction model. The results of the proposed fatigue criterion and fatigue life prediction model are validated with experimental results from the literature.

© 2005 Elsevier Ltd. All rights reserved.

Keywords: High-cycle fatigue; Multiaxial fatigue; Critical plane; Life prediction; Metals

1. Introduction

Many critical mechanical components experience multiaxial cyclic loadings during their service life, such as railroad wheels, crankshafts, axles, and turbine blades, etc. Different from the uniaxial fatigue problem, the multiaxial fatigue problem is more complex due to the complex stress states, loading histories and different orientations of the initial crack in the components. In recent decades, numerous attempts to develop multiaxial fatigue damage criteria and fatigue damage modeling have been reported. Several reviews and comparisons of existing multiaxial fatigue models can be found elsewhere [10,27,36,37].

Although there are many proposed models for multiaxial fatigue damage modeling, most of them are limited to specific materials or loading conditions. Some of them cannot predict the initial crack orientation, which is another distinct characteristic of multiaxial fatigue damage compared with the uniaxial fatigue problem. To the authors' knowledge, no existing multiaxial fatigue damage model is universally accepted.

In this paper, several high-cycle fatigue damage models are first discussed briefly. Then, a new fatigue criterion

based on the critical plane approach is proposed. Unlike the previous critical plane-based models, the critical plane in the current model is theoretically correlated with the fatigue crack initiation plane and also depends on the material properties. This makes the proposed model have almost no limitations in applicability with respect to different metals. Then, a correction factor considering the effect of the mean stress is introduced. The current model is compared with other existing criteria using the available experimental data in the literature. The fatigue criterion is then extended to predict the fatigue life under multiaxial loading conditions. The predicted lives are compared with experimental observations reported in the literature.

2. Existing high-cycle fatigue criteria

Fatigue damage models can be divided into three groups: stress-based models, strain-based models and energy-based models. Since the main focus of this paper is multiaxial high-cycle fatigue, only the stress-based approach is reviewed in this section, which is popularly used in high-cycle fatigue analysis. Large numbers of models are available; only a few of them are briefly discussed here.

The stress-based approaches can be divided into four groups based on empirical equivalent stress, stress invariants, average stress and critical plane stress. Gough and Pollard [11,12] suggested an empirical ellipse formula as a multiaxial fatigue criterion. Sines [29] gave a criterion

* Corresponding author. Tel.: +1 615 322 3040; fax: +1 615 322 3365.
E-mail address: sankaran.mahadevan@vanderbilt.edu (S. Mahadevan).

related to the second invariant of the stress deviator and first invariant of the stress tensor. Langer [19] proposed an equivalent stress based on the Tresca equivalent stress. ASME [1] used modified Langer’s method, using the Von Mises equivalent stress. Lee [20] proposed a modified empirical formula based on Gough’s model. Several different multiaxial fatigue criteria based on stress invariants can be found elsewhere [5,15].

Papadopoulos et al. [27] proposed a fatigue criterion based on the average stress approach, i.e. an average of the stress components involving the critical point, as

$$\begin{aligned} & \sqrt{\langle T_a^2 \rangle} + \lambda[(J_1)_a + (J_1)_m] \\ & = \sqrt{\frac{\sigma_a^2}{3} + \tau_a^2} + \lambda[(J_1)_a + (J_1)_m] = \xi \end{aligned} \quad (1)$$

where $\langle T_a^2 \rangle$ is the average quantity within a volume, σ_a is the bending stress amplitude, τ_a is the torsion stress amplitude, $\lambda = (3t_{-1}/f_{-1} - \sqrt{3})$ and $\xi = t_{-1}$, f_{-1} and t_{-1} are fatigue limits in fully reversed bending and torsion, respectively. J_1 is the first invariant of the stress tensor. The subscripts a and m refer to the stress amplitude value and mean stress value, respectively.

This model is limited to materials, in which t_{-1}/f_{-1} is between 0.577 and 0.8. Another limitation of the model is that non-proportional loading has no effect based on Eq. (1), which is in conflict with experimental observations [37]. Other average stress approaches can be found elsewhere, e.g. Refs. [13,21].

In recent years, criteria based on the critical plane approach for multiaxial fatigue evaluation have been gaining popularity [33,37]. According to the critical plane approach, fatigue evaluation is performed on one plane across a critical location in the component. This plane is called the critical plane, which is usually different for different fatigue models.

Findley [9] proposed a damage parameter based on the linear combination of the shear stress amplitude and maximum normal stress acting on the critical plane. Matake [23] proposed a fatigue criterion based on the critical plane approach, which uses a damage parameter based on the linear combination of the shear stress amplitude and maximum normal stress acting on the critical plane. The orientation of this plane is described by the spherical coordinates (ϕ_c, θ_c) of its unit normal vector n_c . The critical plane is defined as the plane on which the shear stress amplitude achieves the maximum value:

$$\begin{cases} (\phi_c, \theta_c) = \max_{(\phi, \theta)} [\tau_a(\phi, \theta)] \\ \tau_a(\phi_c, \theta_c) + k\sigma_{\max}(\phi_c, \theta_c) = \xi \end{cases} \quad (2)$$

where the subscript c refers to the critical plane. The material constants k and ξ are given as

$$k = (2t_{-1}/f_{-1} - 1); \quad \xi = t_{-1} \quad (3)$$

McDiarmid [24] uses the concept of Case A and Case B cracks (Brown and Miller [38]). Case A cracks propagate along the component surface, while Case B cracks propagate into the surface. The fatigue damage is evaluated on the critical plane corresponding to the two crack cases. The critical plane is defined the same as in Matake’s model (Eq. (2)). The material constants are given as

$$k = \frac{\tau_{A,B}}{2\sigma_u}; \quad \xi = \tau_{A,B} \quad (4)$$

where $\tau_{A,B}$ is the material parameter according to Case A or Case B cracks, σ_u is the ultimate tensile strength of the material.

Carpinteri and Spagnoli [2] proposed a criterion based on the critical plane for hard metals. The calculation of the critical plane is performed by two steps. First, the weighted mean direction of the maximum principal stress is evaluated [3,4]. Then, an empirical formula is used to correlate the above direction to the critical plane. After determining the critical plane, the fatigue criterion is expressed by a non-linear combination of the maximum normal stress and shear stress amplitude acting on the critical plane:

$$\begin{cases} \delta = 45 \frac{3}{2} \left[1 - \left(\frac{t_{-1}}{f_{-1}} \right)^2 \right] \\ \left(\frac{\sigma_{\max}}{f_{-1}} \right)^2 + \left(\frac{\tau_a}{t_{-1}} \right)^2 = 1 \end{cases} \quad (5)$$

where δ is the angle between w_c and l_c in degrees, w_c is the normal vector of the critical plane, l_c is the direction of the weighted mean direction of the maximum principle stress.

Papadopoulos [28] proposed a critical plane model, which uses the average shear stress quantity (named generalized shear stress amplitude) and the maximum value of the hydrostatic stress.

Some of critical plane methods have limitations with respect to the applicability of the material. For the model suggested by Carpinteri and Spagnoli [2], t_{-1}/f_{-1} should be between 0.577 and 1. Another aspect of the critical plane approach is that most of the critical plane definitions only depend on the stress state. Carpinteri and Spagnoli [2] define the critical plane which depends on both the stress state and material properties. The relationship between the fatigue fracture plane and the critical plane is proposed in Section 3.1.

3. Proposed multiaxial fatigue model

3.1. Fatigue fracture plane and critical plane

The definitions of the fatigue fracture plane and the critical plane should be clarified first. Experimental results show that for commonly used metallic materials, fatigue crack first occurs along the crystal slip plane, and then propagates perpendicular to the maximum principal stress

direction. The fatigue fracture plane here refers to the crack plane observed at the macro level. The critical plane is not an actual crack plane. It is a material plane on which the fatigue damage is evaluated. The two planes may or may not coincide with each other. Several authors proposed different methods to predict the fatigue fracture plane. McDiarmid [24] defines the fracture plane as the plane which experiences the maximum principal stress. Carpinteri et al. [3,4] suggest that the fracture plane coincides with the weighted mean principal stress direction. Socie [32] proposed to correlate the fatigue fracture plane to either a Mode I crack or a Mode II growth mechanism. Here, in this paper, the fatigue fracture plane is assumed to be the plane, which experiences the maximum normal stress amplitude.

The critical plane orientation may differ from the fatigue fracture plane for different materials. In this paper, the calculation of the critical plane orientation is derived as below.

3.2. Critical plane and fatigue damage parameter

First consider the fully reversed bending–torsion fatigue problem (with no mean stress). A new fatigue damage parameter is proposed based on the non-linear combination of the normal stress amplitude, shear stress amplitude and hydrostatic stress amplitude acting on the critical plane, as

$$\sqrt{\left(\frac{\sigma_{a,c}}{f_{-1}}\right)^2 + \left(\frac{\tau_{a,c}}{t_{-1}}\right)^2} + k\left(\frac{\sigma_{a,c}^H}{f_{-1}}\right)^2 = \beta \quad (6)$$

where $\sigma_{a,c}$, $t_{a,c}$ and $\sigma_{a,c}^H$ are the normal stress amplitude, shear stress amplitude and hydrostatic stress amplitude acting on the critical plane, respectively. k and β are material parameters which can be determined by uniaxial and torsional fatigue limits.

It is obvious that both shear stress and normal stress contribute to the final failure of mechanical components under multiaxial fatigue loading. However, several researchers have also noticed the importance of hydrostatic stress and included its effect in their model [5,15,27,29]. Therefore, Eq. (6) includes all these stresses in the damage model.

However, the contribution of hydrostatic stress is different for different models and seems to vary with material properties. Therefore, we proposed the new failure criterion in Eq. (6). This equation implies that the final multiaxial fatigue damage is the sum of damage caused by normal stress amplitude, shear stress amplitude (on the critical plane) and the hydrostatic stress amplitude. The coefficient k in Eq. (6) takes this into account, and ensures that the contribution of hydrostatic stress amplitude is different for different materials.

Eq. (6) is a second order combination of the damage caused by different stress components. Since the equivalent stress in Eq. (22), which is derived using Eq. (6), is similar to the Von Mises and Tresca stresses for two special

materials, we use a second order function in the current study. If a different damage parameter were used, a different fatigue damage model could be obtained following the procedure described below.

3.2.1. Case 1

Since the relationship between the critical plane and fatigue fracture plane has not been determined yet, suppose that for one type of material the critical plane coincides with the fatigue fracture plane. In other words, the angle between these two planes is zero.

For a fully reversed uniaxial fatigue experiment ($\sigma_a = f_{-1}$, $\tau_a = 0$), the fatigue fracture plane is perpendicular to the normal stress direction. Thus, we obtain

$$\begin{cases} \sigma_{a,c} = f_{-1} \\ \tau_{a,c} = 0 \\ \sigma_{a,c}^H = f_{-1}/3 \end{cases} \quad (7)$$

For a fully reversed pure torsional fatigue experiment ($\sigma_a = 0$, $\tau_a = t_{-1}$), the fatigue fracture plane has an angle of 45° with the shear stress direction. Thus,

$$\begin{cases} \sigma_{a,c} = t_{-1} \\ \tau_{a,c} = 0 \\ \sigma_{a,c}^H = 0 \end{cases} \quad (8)$$

Substitute Eqs. (7) and (8) to Eq. (6), we can get

$$\begin{cases} \sqrt{1 + \frac{k}{9}} = \beta \\ \sqrt{\left(\frac{t_{-1}}{f_{-1}}\right)^2} = \beta \end{cases} \quad (9)$$

Solve Eq. (9) for material parameters:

$$\begin{cases} k = 9 \left[\left(\frac{t_{-1}}{f_{-1}}\right)^2 - 1 \right] \\ \beta = \frac{t_{-1}}{f_{-1}} \end{cases} \quad (10)$$

Notice that the physical meaning of k is the contribution of damage caused by the hydrostatic stress amplitude. It should be non-negative. So t_{-1}/f_{-1} should not be lower than one. Materials with $t_{-1}/f_{-1} \leq 1/\sqrt{3}$ are usually known as ductile (mild) metals, whereas materials with $1/\sqrt{3} \leq t_{-1}/f_{-1} \leq 1$ are usually known as brittle (hard) metals [2]. Materials with $t_{-1}/f_{-1} \geq 1$ are referred as extremely brittle (hard) metals in this paper. Recall the assumption made before this calculation. If the present damage parameter (Eq. (6)) is adopted, the critical plane could coincide with the fatigue fracture plane only for an extremely brittle material ($t_{-1}/f_{-1} \geq 1$). It is also interesting to notice that k equals zero when $t_{-1}/f_{-1} = 1$, which means (from Eq. (6)) that the hydrostatic stress amplitude has no contribution to the fatigue damage for this material according to the present definition of the damage parameter (Eq. (6)).

3.2.2. Case 2

Now suppose that, for one type of material, the critical plane is 45° off the fatigue fracture plane, which is the maximum shear stress plane for uniaxial and torsional loading. Following the steps described above, the material parameters k and β are once again calculated.

For a fully reversed uniaxial fatigue experiment ($\sigma_a=f_{-1}$, $\tau_a=0$), the stress components on the critical plane are

$$\begin{cases} \sigma_{a,c} = f_{-1}/2 \\ \tau_{a,c} = f_{-1}/2 \\ \sigma_{a,c}^H = f_{-1}/3 \end{cases} \quad (11)$$

For a fully reversed pure torsional fatigue experiment ($\sigma_a=0$, $\tau_a=t_{-1}$), the stress components on the critical plane are

$$\begin{cases} \sigma_{a,c} = 0 \\ \tau_{a,c} = t_{-1} \\ \sigma_{a,c}^H = 0 \end{cases} \quad (12)$$

Substituting Eqs. (11) and (12) in Eq. (6):

$$\begin{cases} \sqrt{\frac{1}{4} + \frac{f_{-1}^2}{4t_{-1}^2} + \frac{k}{9}} = \beta \\ 1 = \beta \end{cases} \quad (13)$$

Solving Eq. (13) for the material parameters, we obtain

$$\begin{cases} k = \frac{9}{4} \left(3 - \left(\frac{f_{-1}}{t_{-1}} \right)^2 \right) \\ \beta = 1 \end{cases} \quad (14)$$

From Eq. (14), t_{-1}/f_{-1} should not be lower than $1/\sqrt{3}$. This type of material ($t_{-1}/f_{-1} \geq 1/\sqrt{3}$) is often known as a brittle (hard) metal. Recall the assumption made before this calculation. By using the damage parameter in Eq. (6), the critical plane could be 45° off the fatigue fracture plane only for brittle metals ($t_{-1}/f_{-1} \geq 1/\sqrt{3}$). Similar to the Case 1, k equals zero when $f_{-1}/t_{-1} = \sqrt{3}$, which means (from Eq. (6)) that the hydrostatic stress amplitude $\sigma_{a,c}^H$ has no contribution to the fatigue damage for this material according to the present definition of the damage parameter.

Several conclusions can be drawn based on the derivations of the critical plane orientations for the two cases above. The contribution of the hydrostatic stress amplitude is different for different materials if the critical plane is fixed for all materials. There are two materials ($t_{-1}/f_{-1} = 1$ and $t_{-1}/f_{-1} = 1/\sqrt{3}$), for which the contribution of the hydrostatic stress amplitude is zero if the critical plane is defined as shown in Case 1 and Case 2. It is also noticed that, if the critical plane is fixed, the range of applicable materials is limited.

3.2.3. General case

Instead of fixing the critical plane, the current model searches for the critical plane orientation on which

the contribution of the hydrostatic stress amplitude is minimized to zero. First, it searches for the plane that experiences the maximum normal stress amplitude, which is assumed to be the fatigue fracture plane in the proposed model. Then, the angle α between the critical plane and the fatigue fracture plane is computed using uniaxial and pure torsional fatigue test results using the same procedure described in the last two sections. Since the contribution of the hydrostatic stress amplitude is zero, Eq. (6) is rewritten as

$$\sqrt{\left(\frac{\sigma_{a,\alpha}}{f_{-1}}\right)^2 + \left(\frac{\tau_{a,\alpha}}{t_{-1}}\right)^2} = \beta \quad (15)$$

The objective is to find α and β for an arbitrary material, following the steps described for the first two cases.

For a fully reversed uniaxial fatigue experiment ($\sigma_a=f_{-1}$, $\tau_a=0$), the fatigue fracture plane is perpendicular to the normal stress direction. The critical plane is at an angle α off the fatigue fracture plane. Thus, we obtain

$$\begin{cases} \sigma_{a,\alpha} = \frac{f_{-1}}{2} \pm \frac{f_{-1}}{2} \cos(2\alpha) \\ \tau_{a,\alpha} = \pm \frac{f_{-1}}{2} \sin(2\alpha) \end{cases} \quad (16)$$

For fully reversed pure torsional fatigue experiment ($\sigma_a=0$, $\tau_a=t_{-1}$), the critical plane is at an angle α degree off the maximum normal stress plane. Thus,

$$\begin{cases} \sigma_{a,\alpha} = \pm t_{-1} \cos(2\alpha) \\ \tau_{a,\alpha} = \pm t_{-1} \sin(2\alpha) \end{cases} \quad (17)$$

Substituting Eqs. (16) and (17) in Eq. (15), we have

$$\begin{cases} \frac{[1 \pm \cos(2\alpha)]^2}{4} + \frac{1}{4} \left(\frac{f_{-1}}{t_{-1}}\right)^2 \sin^2(2\alpha) = \beta^2 \\ \left(\frac{t_{-1}}{f_{-1}}\right)^2 \cos^2(2\alpha) + \sin^2(2\alpha) = \beta^2 \end{cases} \quad (18)$$

Solving Eq. (18) for α and β , we obtain

$$\begin{cases} \cos(2\alpha) = \frac{-2 + \sqrt{4 - 4(1/s^2 - 3)(5 - 1/s^2 - 4s^2)}}{2(5 - 1/s^2 - 4s^2)} \\ \beta = [\cos^2(2\alpha)s^2 + \sin^2(2\alpha)]^{1/2} \end{cases} \quad (19)$$

where $s=(t_{-1}/f_{-1})$ is a material constant. Here, α takes values from 0 to $(\pi/2)$. As shown in Eq. (19), both α and β are functions of the material property s . It needs to be pointed out that α is a material parameter and does not change its value with the ratio and phase difference between normal stress amplitude and shear stress amplitude. It is found that α increases as s decreases. α equals 0 when s equals 1. Mathematically, α equals $(\pi/2)$ when s equals zero. However, this state cannot be achieved in the realistic situation. β does not change monotonically with respect to s , but all the β values are close to 1 for materials with $1/\sqrt{3} < s < 1$.

Table 1
Material parameters for fatigue damage evaluation

Material property	$s = \frac{t_{-1}}{f_{-1}} \leq 1$	$s = \frac{t_{-1}}{f_{-1}} > 1$
α	$\cos(2\alpha) = \frac{-2 + \sqrt{4 - 4(1/s^2 - 3)(5 - 1/s^2 - 4s^2)}}{2(5 - 1/s^2 - 4s^2)}$	$\alpha = 0$
k	$k = 0$	$k = 9(s^2 - 1)$
β	$\beta = [\cos^2(2\alpha)s^2 + \sin^2(2\alpha)]^{1/2}$	$\beta = s$

From Eq. (19), α has no real solution for $s > 1$. This indicates that, for an extremely brittle material, the contribution of hydrostatic stress amplitude cannot be minimized to zero and must be considered during the fatigue damage evaluation. We could use the results in Case 1 for the material with $s > 1$. The summary of material parameters for all types of materials are listed in Table 1.

As a result of the above derivation, the methodology becomes very simple with the current model. For any arbitrary loading history, the fatigue fracture plane is identified on the plane with maximum normal stress amplitude. This is achieved by enumeration, by changing the angle by 1° increment. Then, the angle α and material parameters are determined for different materials according to Table 1. The critical plane is the plane, which has an angle α with the maximum normal stress amplitude plane. Finally, the stress components on the critical plane are calculated and the fatigue damage is evaluated using Eq. (6). Note that the critical plane in the proposed model depends not only on the stress state (maximum normal stress amplitude plane) but also on the material properties (angle α).

3.3. Mean stress effect

Practical mechanical components generally experience cyclic fatigue loading together with the mean stress. The mean stress could also be introduced by residual stress, environmental effects, etc. It is well known that the mean normal stress has an important effect on fatigue life. Normally, tensile mean stress reduces the fatigue life, while compressive mean stress increases the fatigue life [30].

There are many models for mean normal stress effect correction. Gerber [39], Goodman [40], Soderberg [41] and Morrow [42] proposed different correction factors. Kujawski and Ellyin [17] proposed a unified approach to mean stress effect. For the multiaxial fatigue problem, mean normal stress is included in the model in different ways [34] depending on different models. Fatemi and Socie [7] considered the maximum normal stress acting on the critical plane. Papadopoulos et al. (1997) considered the hydrostatic mean stress. Varvani-Farahani [35] used a correction factor based on the mean stress on the critical plane.

In the case of mean shear stress effect, there is still much argument as to the proper way to include this effect. From many experimental observations, Smith [31]

concluded that mean shear stress has little effect on the fatigue life and endurance limit. Sines [29] stated that a superimposed mean static torsion has no effect on the fatigue limit of metals subjected to cyclic torsion. A similar conclusion was also found by Davoli et al. [6]. The mean shear stress effect is often neglected in the high-cycle fatigue analysis [6]. Therefore, in the current model, the mean shear stress is also assumed to have no effect on the fatigue criterion and fatigue life in high-cycle fatigue regime.

Based on the experimental data collected from the literature, the mean stress is introduced into the fatigue model by a correction factor $(1 + \eta(\sigma_{m,c}/f_{-1}))$. Thus, Eq. (6) is rewritten as

$$\sqrt{\left[\frac{\sigma_{a,c} \left(1 + \eta \frac{\sigma_{m,c}}{f_{-1}}\right)}{f_{-1}}\right]^2 + \left(\frac{\tau_{a,c}}{t_{-1}}\right)^2 + k \left(\frac{\sigma_{a,c}^H}{f_{-1}}\right)^2} = \beta \quad (20)$$

where η is a material parameter, which can be calibrated using uniaxial fatigue tests with mean stress. For different materials considered in this paper, η ranges from 0.6 to 1.3. If fatigue tests with mean stress are not available, a simplified function (Eq. (21)) is suggested. The experimental value and the simplified formula of η are plotted in Fig. 1.

$$\begin{cases} \eta = \frac{3}{4} + \frac{1}{4} \left(\frac{\sqrt{3} - \frac{f_{-1}}{t_{-1}}}{\sqrt{3} - 1} \right) & \left(\frac{t_{-1}}{f_{-1}} \leq 1 \right) \\ \eta = 1 & \left(\frac{t_{-1}}{f_{-1}} \geq 1 \right) \end{cases} \quad (21)$$

3.4. Fatigue life model

After developing the fatigue limit criterion as above, the methodology for fatigue life prediction is relatively easy. Notice that the fatigue limit is often referred to the fatigue strength at very high-cycle regime (usually 10^6 – 10^7 cycles). For finite fatigue life predictions, the damage parameter

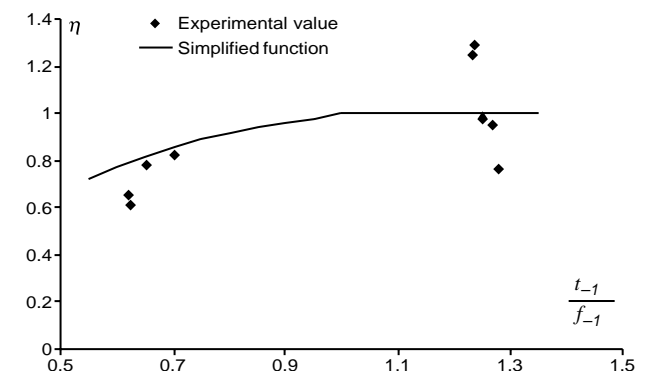


Fig. 1. Experimental values and simplified values of mean stress factor η .

should be correlated with the life (number of loading cycles to failure). Eq. (20) can be rewritten as

$$\frac{1}{\beta} \sqrt{\left[\sigma_{a,c} \left(1 + \eta \frac{\sigma_{m,c}}{f_{-1}} \right) \right]^2 + \left(\frac{f_{-1}}{t_{-1}} \right)^2 (\tau_{a,c})^2 + k(\sigma_{a,c}^H)^2} = f_{-1} \tag{22}$$

The left side of Eq. (22) can be treated as the equivalent stress amplitude. It can be used to correlate with the fatigue life using the uniaxial *S-N* curve. Thus, the fatigue life model is expressed as

$$\frac{1}{\beta} \sqrt{\left[\sigma_{a,c} \left(1 + \eta_{N_f} \frac{\sigma_{m,c}}{f_{N_f}} \right) \right]^2 + \left(\frac{f_{N_f}}{t_{N_f}} \right)^2 (\tau_{a,c})^2 + k(\sigma_{a,c}^H)^2} = f_{N_f} \tag{23}$$

and

$$\begin{cases} \eta_{N_f} = \frac{3}{4} + \frac{1}{4} \left(\frac{\sqrt{3} - f_{N_f}}{t_{N_f}} \right) & (f_{N_f} > 1) \\ \eta_{N_f} = 1 & (f_{N_f} \leq 1) \end{cases} \tag{24}$$

where N_f is the number of cycles to failure. Notice here f_{-1} and t_{-1} in Eq. (20) and Eq. (21) change to f_{N_f} and t_{N_f} , respectively, which are fatigue strength coefficients at finite life N_f for uniaxial and torsional loadings. Eq. (23) has no closed form solution. In practical calculation, a trial and error method can be used to find N_f . For high-cycle fatigue, f_{N_f} and t_{N_f} take initial values as f_{-1} and t_{-1} . It is found that usually a few iterations are enough to make N_f converge. Eqs. (23) and (24) together with the parameters in Table 1 are used for fatigue life prediction in the following. The quantity s in Table 1 is redefined as $s = \frac{t_{N_f}}{f_{N_f}}$.

4. Validation of the fatigue model

4.1. Validation of the fatigue criterion

Two sets of bending and torsion experimental fatigue limit data are used in this section to validate the current fatigue criterion. The first one contains four different materials [27]. Some material properties are reported in Table 2. The error index of the current model is compared with three other models: Mataka's, McDiarmid's, and

Table 2
Material properties of the test specimens employed by Papadopoulos et al. [27]

Material	f_{-1} (MPa)	t_{-1} (MPa)	t_{-1}/f_{-1}	σ_u (MPa)
Hard steel	313.9	196.2	0.63	680
42CrMo4	398	260	0.65	1025
34Cr4	410	256	0.62	795
30NCD16	660	410	0.62	1880

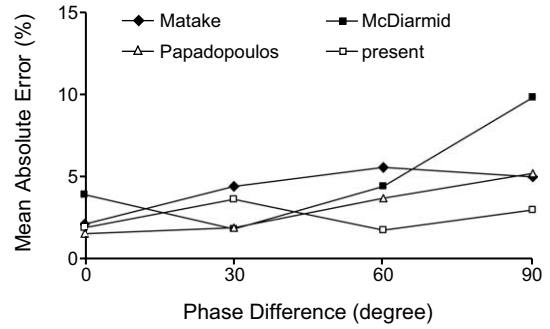


Fig. 2. Mean absolute error comparisons under different phase differences for hard steel.

Papadopoulos's [23,24,27]. The error index is defined same as in Papadopoulos et al. [27]: the relative difference between the left and right hand sides of each criterion.

$$I = \frac{\text{left hand side} - \text{right hand side}}{\text{left hand side}} (\%) \tag{25}$$

The experimentally observed fatigue fracture plane orientations are not reported by Papadopoulos et al. [27]. Only the experimental fatigue limit data are compared with the model predictions. The main objective of the comparison is to find the model's applicability to different materials and loading conditions. So the comparisons here are performed using the mean absolute error for different phase differences according to different materials through Figs. 2–5.

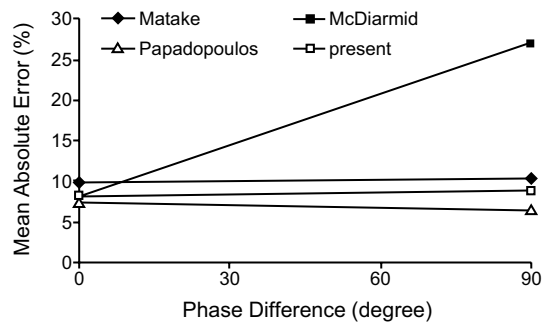


Fig. 3. Mean absolute error comparisons under different phase differences for 42CrMo4.

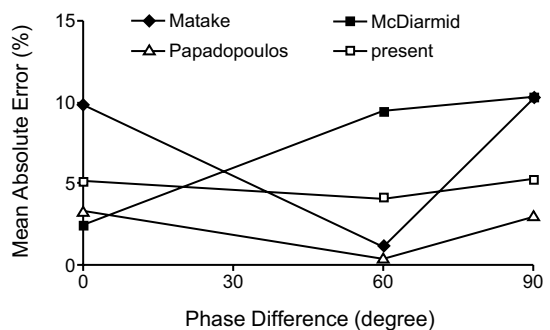


Fig. 4. Mean absolute error comparisons under different phase differences for 34Cr4.

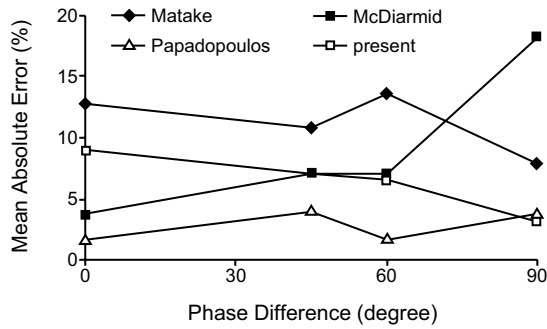


Fig. 5. Mean absolute error comparisons under different phase differences for 30NCD16.

In Figs. 2–5, it is seen that both Papadopoulos’ model and the present model give us a good estimation of the fatigue limit. For some materials, the results of the present model give slightly smaller errors; for others, Papadopoulos’ results are better. Both Matake’s model and McDiarmid’s model give a relatively larger error. It also seems that the error in McDiarmid’s model increases as the phase difference increases. Notice that the t_{-1}/f_{-1} values of all the materials fall into a very small range (0.62–0.65, Table 2), making it difficult to predict the performance of the models for other materials outside this narrow range.

Another set of experimental data [2] is used to test the model’s performance for different materials. The material properties are listed in Table 3. It should be noted that the experimental work for hard steel in Table 2 is exactly the same as that for hard steel in Table 3. This was originally done by Nishihara and Kawamoto [26]. Different other fatigue limit data have been reported by several authors. Papadopoulos et al. [27] uses the data reported by McDiarmid [24]. Carpinteri and Spagnoli [2] use the data reported by Macha [22]. In order to diminish the data estimation error introduced by different authors, both data sets are used here.

The fatigue fracture plane orientation is reported by Macha [22]. The comparisons of the fatigue fracture orientations between experimental observations and present model predictions are listed together in Table 4. The present model predictions of the fatigue fracture orientation agree with the experimental observations very well. Although not listed in this paper, both McDiarmid’s model and Carpinteri’s model gave almost the same predictions as the current model.

The comparisons of the fatigue limits for different models are plotted in Figs. 6–8. Since Matake’s model fails to determine the critical plane under some loading cases,

Table 3
Material properties of the test specimens employed by Carpinteri and Spagnoli [2]

Material	f_{-1} (MPa)	t_{-1} (MPa)	t_{-1}/f_{-1}	σ_u (MPa)
Hard steel	313.9	196.2	0.63	704.1
Mild steel	235.4	137.3	0.58	518.8
Cast iron	96.1	91.2	0.95	230.0

Table 4
Comparisons of fatigue fracture orientations between experimental observations and model predictions

Hard steel			Mild steel			Cast iron		
Test number	θ_{exp} (°)	θ_{cal} (°)	Test number	θ_{exp} (°)	θ_{cal} (°)	Test number	θ_{exp} (°)	θ_{cal} (°)
1	0	0	1	0	0	1	0	0
2	12	11	2	12	11	2	12	11
3	22	22	3	22	22	3	25	22
4	34	34	4	30	34	4	34	34
5	45	45	5	45	45	5	49	45
6	16	22	6	12	18	6	0	0
7	32	34	7	8	35	7	0	0
8	8	18	8	0	0	8	37	39
9	22	35	9	8	0			
10	0	0	10	39	39			
11	0	0						
12	28	39						

Carpinteri and Spagnoli’s model is used in the current comparison.

From Figs. 6–8, both Carpinteri’s model and the present model give an overall small error. McDiarmid’s model gives a poor estimation for cast iron. Papadopoulos’ model seems to have an increased error as the phase difference increases, especially for cast iron. It is interesting to remark that Carpinteri’s model and the present model give very close predictions for all the material and loading conditions. For the experimental data used by Carpinteri and Spagnoli [2], mean stress is zero and t_{-1}/f_{-1} is less than one.

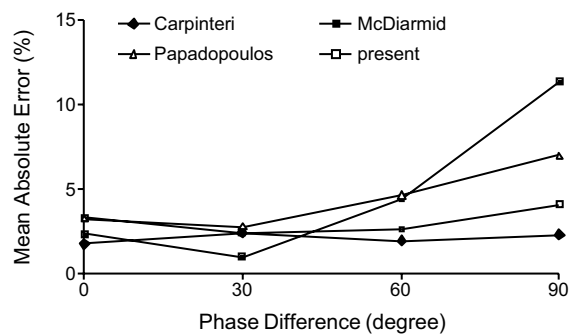


Fig. 6. Mean absolute error comparisons under different phase differences for hard steel.

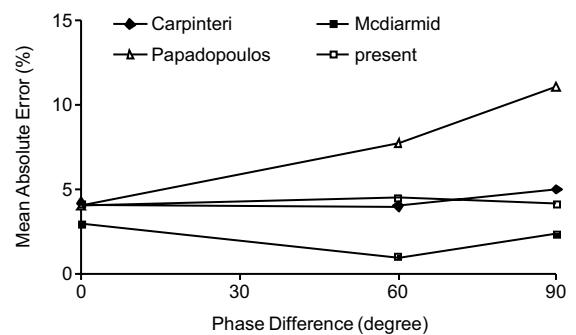


Fig. 7. Mean absolute error comparisons under different phase differences for mild steel.

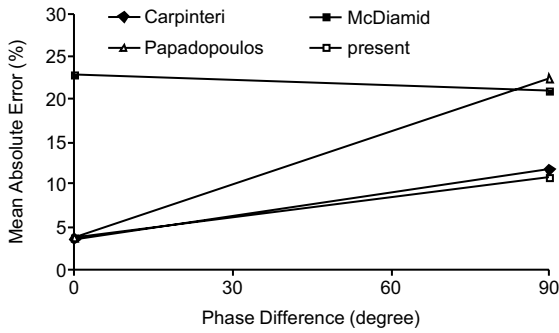


Fig. 8. Mean absolute error comparisons under different phase differences for cast iron.

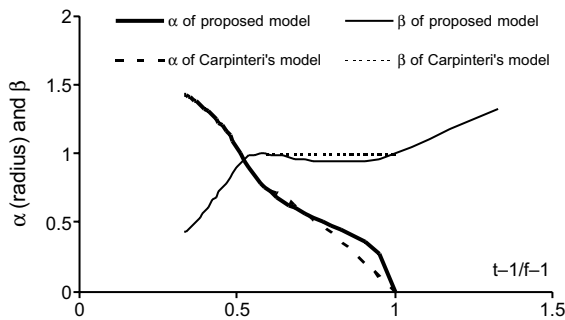


Fig. 9. Comparison of the material parameters for present model and Carpinteri's model.

Their criterion (Eq. (5)) is rewritten as

$$\begin{cases} \alpha = 45 \frac{3}{2} \left[1 - \left(\frac{t_{-1}}{f_{-1}} \right)^2 \right] \\ \sqrt{\left(\frac{\sigma_{a,c}}{f_{-1}} \right)^2 + \left(\frac{\tau_{a,c}}{t_{-1}} \right)^2} = \beta = 1 \end{cases} \quad (26)$$

The present model (Eq. (20)) can be rewritten as

$$\begin{cases} \cos(2\alpha) = \frac{-2 + \sqrt{4 - 4(1/s^2 - 3)(5 - 1/s^2 - 4s^2)}}{2(5 - 1/s^2 - 4s^2)} \\ \sqrt{\left(\frac{\sigma_{a,c}}{f_{-1}} \right)^2 + \left(\frac{\tau_{a,c}}{t_{-1}} \right)^2} = \beta \end{cases} \quad (27)$$

Since the fatigue fracture planes predicted by the two models are almost the same, the only small differences between the two criteria are the material parameters α and β , plotted in Fig. 9. As is shown in Fig. 9, it is found that the two sets values of the material parameters α and β are close for hard metals ($1/\sqrt{3} < t_{-1}/f_{-1} < 1$), especially for the materials used by Carpinteri and Spagnoli [2]. Thus, the two models give very close results in this case. Carpinteri and Spagnoli's model cannot be applied to extreme brittle metals ($t_{-1}/f_{-1} > 1$) and ductile metals ($t_{-1}/f_{-1} < 1/\sqrt{3}$), because the critical plane is not defined in those ranges by the above authors.

4.2. Validation of the fatigue life prediction model

Four sets of fatigue experimental data are employed in this section: SAE-1045-1 steel reported by Kurath et al. [18]; SAE-1045-2 steel reported by Fatemi and Stephens [8]; SM45C steel reported by Lee [20]; 5% chrome work roll steel reported by Kim et al. [16]. Some material axial and torsion fatigue properties are listed in Table 5.

Notice that the present model has no special requirement of the $S-N$ curve format. Different formats can be used for best regression results. The R^2 values are also listed in Table 5. The four materials cover a wide range of steels, from extremely brittle steel to ductile steel (t_{-1}/f_{-1} ranges from 0.57 to 1.28). The comparisons of the present model predictions and experimental observations are plotted together in Figs. 10–13. Two bounds are also plotted. The inner bound is according to the life factor of 2, whereas the outer bound is according to the life factor of 3.

From Figs. 10–13, it can be found that the proposed model results agrees with the experimental observations very well. Seventy eight percent of the total points fall into the range of life factor 2 and ninety two percent of the total points fall into the range of life factor 3. There are no systemic errors for the loading conditions, material properties and mean stress effect in the present model. The error index is defined as the relative difference from the experimental observations. The histogram of the error index considering all the experimental specimens is plotted in Fig. 14.

The worst case of the proposed model's life prediction is for 5% chrome work roll steel. As mentioned by Kim et al.

Table 5
Material fatigue properties of four different steels

Material	Fully reversed $S-N$ curve		R^2	Fatigue limits (MPa)	(t_{-1}/f_{-1})
SAE-1045-1	Axi.	$\sigma_a = 1261.8(\text{Log}(N))^{-0.9315}$	0.98	237.76	0.61
	Tor.	$\sigma_a = 603.33(\text{Log}(N))^{-0.8303}$	0.98	136.29	
SAE-1045-2	Axi.	$\sigma_a = 1248.7(\text{Log}(N))^{-0.9157}$	0.99	242.05	0.57
	Tor.	$\sigma_a = 558.84(\text{Log}(N))^{-0.7402}$	0.98	148.35	
SM45C	Axi.	$\sigma_a = 445.75 + \frac{378.25}{1 + \left(\frac{\text{Log}(N)}{4.23}\right)^{8.25}}$	0.99	445.75	0.71
	Tor.	$\sigma_a = 317.12 + \frac{158.63}{1 + \left(\frac{\text{Log}(N)}{3.60}\right)^{9.30}}$	0.99	317.12	
5% chrome work roll steel	Axi.	$\sigma_a = 125.46 \text{Log}(N) + 1256.8$	0.99	504.04	1.28
	Tor.	$\sigma_a = -145.3 \text{Log}(N) + 1515.8$	0.91	644.00	

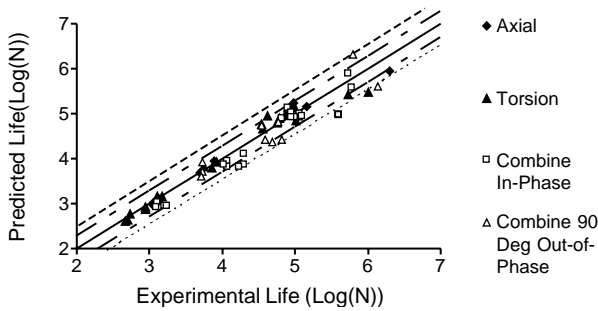


Fig. 10. Comparisons of life predictions and experimental observations for SAE-1045-1.

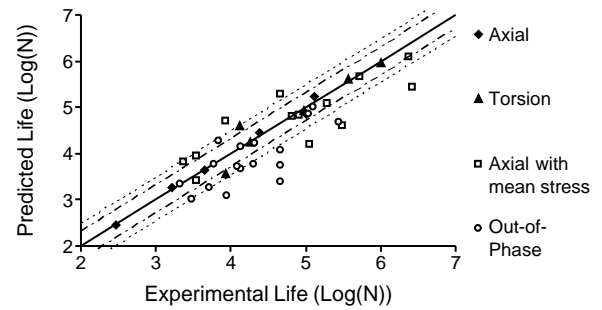


Fig. 13. Comparisons of life predictions and experimental observations for 5% chrome work roll steel.

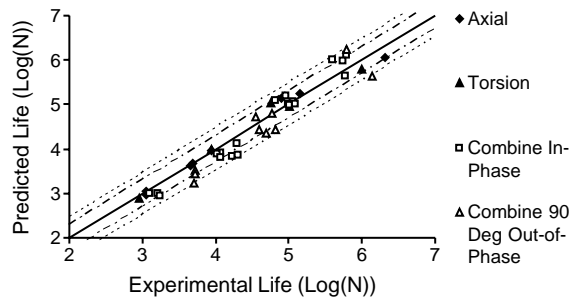


Fig. 11. Comparisons of life predictions and experimental observations for SAE-1045-2.

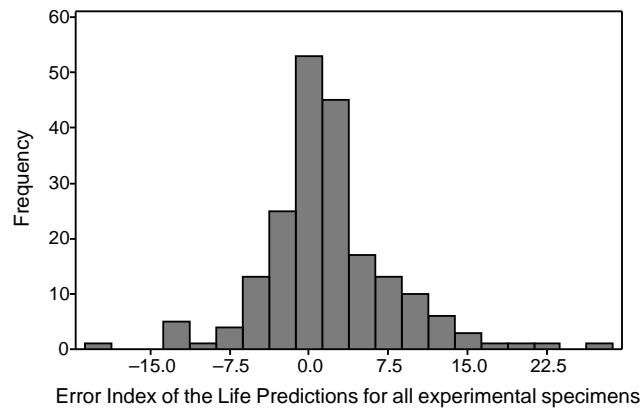


Fig. 14. Histogram of the error index of fatigue life (log scale) considering all experimental specimens.

[16], there is more scatter in life data than usually observed in the laboratory for ductile metals. This is believed to be an inherent characteristic of materials whose life is controlled by defects [14,25]. Despite the larger scatter, the proposed model predicts the trend very well. The fatigue fracture plane orientations are also reported by Kim et al. [16]. The present model predictions and experimental observations are listed in Table 6.

5. Conclusion

A new multiaxial fatigue criterion is developed in this paper. The predictions based on the current criterion show good agreement with the fatigue limit experimental data

reported in the literature. The new multiaxial fatigue criterion is then extended to a multiaxial fatigue life prediction model for constant amplitude, in-phase and out-of-phase loading conditions. Four sets of experimental fatigue life data under proportional and non-proportional loading conditions are used to validate the current methodology, which cover a wide range of metals. A very good agreement is obtained both for fatigue life predictions and fatigue fracture plane orientation predictions.

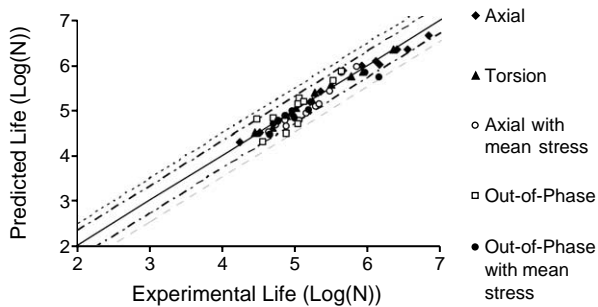


Fig. 12. Comparisons of life predictions and experimental observations for SM45C.

Table 6
Comparisons of fatigue fracture orientations between experimental observations and model predictions for 5% chrome work roll steel reported by Kim et al. [16]

Test number	θ_{exp} (°)	θ_{cal} (°)	Test number	θ_{exp} (°)	θ_{cal} (°)
1	25	24	11	10	17
2	10	21	12	170	163
3	172	173	13	39	32
4	31	32	14	32	34
5	25	33	15	35	34
6	143	146	16	40	38
7	41	37	17	31	34
8	40	38	Uniaxial	0	0
9	135	139	Torsion	45	45
10	21	24			

The current fatigue model is a critical plane-based model. Most of the earlier models based on the critical plane approach assume that the critical plane only depends on the stress state. This indicates that such models account the fatigue damage accumulation in the same way for different materials under the same stress state. Their applicability generally depends on the material's properties. In the current model, the critical plane does not only depend on the stress state but also on the material properties. The critical plane is theoretically determined by minimizing the damage introduced by the hydrostatic stress amplitude, which makes the proposed model have almost no applicability limitations with respect to different metals. Data on a wide range of metals, from extremely brittle steels to ductile steels, are chosen to validate the current model. It is shown that there are no systematic errors according to material properties and loading conditions.

There are some other advantages of the current model. The fatigue fracture plane is also determined and directly related to the critical plane. The calculation is relatively simple. In the fatigue life prediction model, no special requirements are needed for the $S-N$ curve function. The users can choose any $S-N$ curve functions for the best regression results. The mean stress effect is also included in the current model through a general mean stress effect correction factor. The factor can be calibrated using experimental fatigue test data with mean stress. Otherwise the empirical formula suggested by the present authors, may be used.

At present, the proposed model is applicable to multi-axial constant amplitude loading. Further work is needed to extend the current model to general multi-axial random loading.

Acknowledgements

The authors appreciate the help from Brant Stratman, graduate student at Vanderbilt, in data collection.

References

- [1] ASME. Cases of ASME boiler and pressure vessel code, code case N-47-12. New York: American Society of Mechanical Engineers; 1979.
- [2] Carpinteri A, Spagnoli A. Multiaxial high-cycle fatigue criterion for hard metals. *Int J Fatigue* 2001;23:135–45.
- [3] Carpinteri A, Macha E, Brighenti R, Spagnoli A. Expected fracture plane for multiaxial random stress state. Part I. Theoretical aspects of the weight function method. *Int J Fatigue* 1999;21:83–8.
- [4] Carpinteri A, Macha E, Brighenti R, Spagnoli A. Expected fracture plane for multiaxial random stress state. Part II. Numerical simulation and experimental assessment through the weight function method. *Int J Fatigue* 1999;21:89–96.
- [5] Crossland B. Effect of large hydrostatic pressures on the torsional fatigue strength of an alloy steel. In: Proceedings of the international conference on fatigue of metals, Institution of Mechanical Engineers, London; 1956. p. 138–49.
- [6] Davoli P, Bernasconi A, Filippini M, Foletti S, Papadopoulos IV. Independence of the torsional fatigue limit upon a mean shear stress. *Int J Fatigue* 2003;25(6):471–80.
- [7] Fatemi A, Socie DF. A critical plane approach to multiaxial fatigue damage including out of phase loading. *Fatigue Fract Eng Mater Struct* 1988;11:149–65.
- [8] Fateri A, Stephens RI. Biaxial fatigue of 1045 steel under in-phase and 90 deg out-of-phase loading conditions. In: Leese GE, Socie DF, editors. *Multiaxial fatigue: analysis and experiments*, SAE, AE-14. Warrendale, PA: SAE; 1989. p. 121–38.
- [9] Findley WN. A theory for the effect of mean stress on fatigue of metals under combined torsion and axial load or bending. *J Eng Ind, Trans ASME* 1959;81(4):301–6.
- [10] Garud YS. Multiaxial fatigue: a survey of the state-of-the-art. *J Test Eval* 1981;9(3):165–78.
- [11] Gough HJ, Pollard HV. The strength of metals under combined alternating stress. *Proc Inst Mech Eng* 1935;131:3–18.
- [12] Gough HJ, Pollard HV, Clenshaw WJ. Some experiments on the resistance of metals to fatigue under combined stresses. *Aeronautical research council reports, R and M 2522*. London: HMSO; 1951.
- [13] Grubic V, Simburger A. Fatigue under combined out-of-phase multiaxial stresses. *International conference on fatigue, testing and design*. vol. 27. London: Society of Environmental Engineers; 1976. p. 1–27.
- [14] Hanlon DN, Rainforth WM, Sellars CM. The effect of processing route, composition and hardness on the wear resistance of chromium bearing steels in a rolling-sliding configuration. *Wear* 1997;220–9.
- [15] Kakuno H, Kawada Y. A new criterion of fatigue strength of a round bar subjected to combined static and repeated bending and torsion. *Fatigue Eng Mater Struct* 1979;2(2):229–36.
- [16] Kim KS, Nam KM, Kwak GJ, Hwang SM. A fatigue life model for 5% chrome work roll steel under multiaxial loading. *Int J Fatigue* 2004; 26(7):683–9. February.
- [17] Kujawski D, Ellyin F. A unified approach to mean stress effect on fatigue threshold conditions. *Int J Fatigue* 1995;17(2):101–6.
- [18] Kurath P, Downing SD, Galliard D. Summary of non-hardened notched shaft round robin program. In: Leese GE, Socie DF, editors. *Multiaxial fatigue: analysis and experiments*, SAE, AE-14. Warrendale, PA: SAE; 1989. p. 12–32.
- [19] Langer BF. In: Nichols RW, editor. *Design of pressure vessels involving fatigue, pressure vessel engineering*. Amsterdam: Elsevier; 1979. p. 59–100.
- [20] Lee S-B. Out-of-phase bending and torsion fatigue of steels. In: Brown MW, Miller KJ, editors. *Biaxial and multiaxial fatigue*, EGF3. London: Mechanical Engineering Publications; 1989. p. 612–34.
- [21] Liu J, Zenner H. Berechnung der Dauerschwingfestigkeit bei mehrachsiger Beanspruchung. *Mat-wiss u Werkstofftech* 1993;24: 240–9.
- [22] Macha E. Simulation investigations of the position of fatigue fracture plane in materials with biaxial loads. *Mat-wiss u Werkstofftech* 1989; 20:132–6 (see also p. 153–63).
- [23] Mataka T. An explanation on fatigue limit under combined stress. *Bull JSME* 1977;20:257–63.
- [24] McDiarmid DL. Fatigue under out-of-phase bending and torsion. *Fatigue Eng Mater Struct* 1987;9(6):457–75.
- [25] Nadot Y, Mendez J, Ranganathan N, Beranger S. Fatigue life assessment of nodular cast iron containing casting defects. *Fatigue Fract Eng Mater Struct* 1999;22:289–300.
- [26] Nishihara T, Kawamoto M. The strength of metals under combined alternating bending and torsion with phase difference. *Mem College Eng, Kyoto Imper Univ* 1945;11(5):85–112.
- [27] Papadopoulos IV, Avoli P, Gorla C, Filippini M, Bernasconi A. A comparative study of multiaxial high-cycle fatigue criteria for metals. *Int J Fatigue* 1997;19(3):219–35.

- [28] Papadopoulos IV. Long life fatigue under multiaxial loading. *Int J Fatigue* 2001;23(10):839–49.
- [29] Sines G. Behaviour of metals under complex stresses. In: Sines G, Waisman JL, editors. *Metal fatigue*. New York: McGraw-Hill; 1959. p. 145–69.
- [30] Sines G. The prediction of fatigue fracture under combined stresses at stress concentrations. *Bull Jpn Soc Mech Eng* 1961;4(15):443–53.
- [31] Smith JO. Effect of range of stress on fatigue strength of metals. Univ Illinois, Eng Exp Station, Bull No. 334; 1942.
- [32] Socie D. Low-cycle fatigue and elasto-plastic behaviour of materials. In: Rie KT, editor. *Multiaxial fatigue assessment*. UK: Elsevier Applied Science; 1987. p. 465–72.
- [33] Socie D. A summary and interpretation of the society of automotive engineers' biaxial testing program. In: *Multiaxial fatigue: analysis and experiments*. Warrendale, PA: Society of Automotive Engineers, SAE. AE-14; 1989. p. 1–11.
- [34] Socie D, Marquis G, editors. *Multiaxial fatigue*. Society of Automotive Engineers; 2000.
- [35] Varvani-Farahani AA. New energy-critical plane parameter for fatigue life assessment of various metallic materials subjected to in-phase and out-of-phase multiaxial fatigue loading conditions. *Int J Fatigue* 2000;22(4):295–305.
- [36] Wang YY, Yao WX. Evaluation and comparison of several multiaxial fatigue criteria. *Int J Fatigue* 2004;26(1):17–25.
- [37] You BR, Lee SB. A critical review on multiaxial fatigue assessments of metals. *Int J Fatigue* 1996;18(4):235–44.
- [38] Brown MW, Miller KJ. Two decades of progress in the assessment of multiaxial low-cycle fatigue life. In: Amzallag C, Leis B, Rabbe P, editors. *Low-cycle fatigue and life prediction*, ASTM STP 770. Philadelphia, PA: ASTM; 1982. p. 482–99.
- [39] Gerber H. Bestimmung der zulässigen Spannungen in Eisenkonstruktionen. *Zeitschrift des Bayerischen Architekten und Ingenieur-Vereins* 1874;6:101–10.
- [40] Goodman J. *Mechanics applied to engineering*. London: Longmans Green; 1899.
- [41] Soderberg CR. Factor safety and working stress. *Transactions of ASME*, 1939;52:13–28.
- [42] Morrow JD. *Fatigue design handbook-Advances in Engineering*, vol. 4, sec. 3.2. Warrendale, PA: Society of Automotive Engineers; 1968, p. 21–9.